Morphology of Water-Blown Flexible Polyurethane Foams

JAMES PAUL ARMISTEAD and GARTH L. WILKES, *Department of Chemical Engineering and Polymer Materials and Interfaces Laboratory, Virginia Polytechnic Institute and State University, Blacksburg, Virginia 24061-6496,* and ROBERT B. TURNER, *Urethanes, Polymers & Product Research, Dow Chemical Company, Freeport, Texas 77541*

Synopsis

A series of four TDI–polypropylene oxide (PO) water-blown flexible polyurethane foams was produced in which the water content was varied from 2 to 5 pph at a constant isocyanate index of 110. A portion of each foam was thermally compression molded into a plaque. The morphology of both the foams and plaques was investigated using dynamic mechanical spectroscopy (DMS), differential scanning calorimetry (DSC), transmission electron microscopy (TEM), scanning electron microscopy (SEM), swelling, wide angle X-ray scattering (WAXS), and small angle X-ray scattering (SAXS). A high degree of microphase separation occurs in these foams, and its degree is nearly independent of water (hard segment) content. In the foam with the lowest water content the morphology possesses many similarities to that of typical linear segmented urethane elastomers. Small hard segment domains are present with a correlation distance of about 7.0 nm. When the water content is increased a binodal distribution of hard segment material appears. There are the small hard segment domains typical of segmented urethane elastomers as well as larger "hard aggregates" greater than 100 nm in size. The larger domains are thought to be aggregates of rich polyurea that develop by precipitation during the foaming reaction. WAXS patterns of the foams suggest urea and possibly hard segment ordering that may be of a paracrystalline nature but certainly lacking in true 3-dimensional crystallinity.

INTRODUCTION

A typical formulation for a flexible slabstock foam consists of a polyol, water, isocyanate, catalysts, and surfactant. The polyol is usually a trifunctional polyether with an equivalent weight of 500–2000. The isocyanate is generally an 80 : 20 mixture of the 2,4- and 2,6-isomers of toluene diisocyanate. Tin and tertiary amine catalysts are used to accelerate and balance the competing reactions that occur in the foam making process. Surfactants are used to stabilize the rising foam and to assure uniform cell sizes.

There are two primary reaction schemes in foam making. The first is the reaction of a hydroxyl group with an isocyanate group to form an urethane linkage. This reaction joins oligomers and is said to "gel" the foam mix. The second is the reaction of one part water with two parts isocyanate. Water reacts with an isocyanate group to form an unstable carbamic acid which decomposes into an amine and carbon dioxide. The amine then reacts with another isocyanate group to form a urea linkage. This sequence of reactions "blows" the foam mix and chain extends polyurea segments.

Journal of Applied Polymer Science, Vol. 35, 601–629 (1988)
 CCC 0021-8995/88/030601-29$04.00

The foam is made by vigorously mixing the formulation components and pouring them into a walled container. The foam mix rises with the release of carbon dioxide from the "blowing" reaction and is stabilized by the increasing viscosity from the "gelling" reaction. Within 1–3 min the foam mix undergoes a 75–150°C exotherm and rises to the height at which cell rupture occurs. At cell rupture, if the foam has not gelled enough, it will collapse. If it has gelled too much, it will shrink or "prune." Foams which are stable after cell rupture must cure for up to several days before mechanical properties stabilize.

The mechanical properties of a cured foam depend both on the macroscopic cell structure of the foam and the morphology of the material comprising the cell struts. Any change in the formulation of a foam will change both the cell structure and the morphology of the cell struts, so there is no way to evaluate the influence of one independent of the other. Some researchers have isolated material properties from cell structure by studying thermally compressed foams. Compressed foams or "plaques" have been made by thermal compression molding of cured foams[1] and by compressing foams just after cell rupture and allowing them to cure in solid form.[2-4] In both methods, however, the thermal histories of the plaques are different from those of the foam. This is thought to possibly cause significant morphological differences relative to the uncompressed foam, although little proof exists to suggest this hypothesis one way or the other.

The morphology comprising the cell structure or a portion thereof is believed to be generally phase separated somewhat as in thermoplastic elastomers based on SAXS studies.[5] However, phase separation in foams is partially restricted compared to the typical MDI–butane diol segmented elastomers by the use of tri- or higher functional polyols or isocyanates, as well as by possible formation of biurets and allophanates to disrupt hard segment packing. The common use of a mixture of TDI isomers is believed to eliminate hard segment crystallization as can occur in many segmented elastomers that may utilize symmetric diisocyanate moieties. The phase separation issue for a foam is further clouded by the fact that chain extension and gelling occur simultaneously in the foam making process. The focus of much recent work is the sequence of reactions during the manufacture of conventional slabstock foam. These studies bring out the possibility of the precipitation of a urea phase well before gelling is complete and is therefore important to an investigation of the morphology of these systems.

The sequence of foaming reactions has been studied by a number of investigators using FTIR.[6-10] All investigators have observed a growing urea carbonyl absorption at 1715 wavenumbers early in the reaction. When about half of the foam rise height (80°C) was reached, this peak shifted to 1640 wavenumbers and continued to grow. Model studies on diphenyl urea indicated that in good solvents the urea carbonyl absorption was observed at 1715 wavenumbers, and in poor solvents it was observed at 1640 wavenumbers.[6] Based on this information, this suggests that in the formation of polyurethane foams, a point is reached at which the developing polyurea is no longer soluble in the foam mix and precipates out.

FTIR investigations have also revealed important facts about the sequence of reactions. Hauptman et al. and Zarkov et al. showed that the water–TDI reaction is the limiting factor in the blowing and chain extension reaction

sequence and not the decomposition of carbamic acid or the amine–TDI reaction.[6,8] Hauptman et al. also reported no traces of allophanate or biuret formation before the foam mix reached 80°C. Bailey and Critchfield noted that the relative absorbance of urea quickly increased within the first 5 min after mixing (typically the foam rise time is about 2–3 min) and then remained constant.[7] The relative absorbance of urethane increased more slowly after the first 5 or 10 min but then continued to increase at a slow and steady rate for at least 30 more min. Though the measurements were not quantitative, it can be said that urea formation took place more quickly and essentially stopped and that significant urethane formation took place for at least 40 min after mixing. Rossmy and co-workers confirmed the unimportance of urethane formation in the early part of foam formation by synthesizing foams with reactive and nonreactive polyols and by analyzing the unreacted components sampled and quenched at various times during the reaction.[10] Plots of foam temperature vs. foam height for the foams made with reactive and unreactive polyols were nearly identical, indicating that the heat generated by urethane formation early in the reaction is negligible. The ratio of isocyanate group to water consumption was 2 : 1 in the early part of foam formation as required by the blowing and chain extension reaction sequence, also indicating that urethane formation is not significant in the early stages of the reaction.

Van Gheluwe and LeRoux studied the sequence of reactions in polyurethane foams by measuring the temperature of the foam versus time and the change in temperature or first derivative with time.[11] In every foam formulation studied, two maxima were observed in the temperature–time derivative plots. By modifying the reactivity of the polyols and changing catalyst concentrations, they were able to assign the early peak to a maximum rate of the urea reaction and the latter peak to a maximum rate of the urethane reaction. This again shows the predominance of urea formation in the early stages of foam formation.

Rowton reported a simple, qualitative technique for measuring the rigidity of a rising foam.[12] The test is called a BB-drop test and consists of dropping BB's into the rising foam at different time intervals from a fixed height above the rising foam surface. When the foam has cured, it is cut open and the height of the BB above the bottom is an indicator of the integrity of the foam when the BB was dropped. Bailey and Critchfield used this technique in conjunction with their FTIR work.[7] The BB's sank through the rising foam until the precipitation of urea occurred. Then the dropped BB's were supported by the foam indicating that the integrity of the foam was sharply increased by urea precipitation.

Rossmy and co-workers investigated the urea precipitation phenomenon in greater detail.[9,10,13–15] By adding a defoaming agent to a foam formulation they showed that urea precipitation turned a clear foam-mix opaque. No analysis of the precipitate was reported. The temperature of urea precipitation increase with water content, increasing the TDI index, and increasing 2,4-isomer content. These changes all increase the reactivity of the foam mix, and this could explain the higher urea precipitation temperatures. They also noted that cell rupture always occurred just after urea precipitation. In light of these observations they hypothesized that precipitation of polyurea desta-

bilizes the foam mix and leads to cell opening. The surfactant aids in stabilizing the foam by incorporating the urea precipitate into the foam matrix. This adds integrity to the foam.

From the above remarks extending from a literature survey, it is clear that the sequence of foaming reactions imply that urea precipitation occurs during foam manufacture resulting in a two-phase system. In spite of this not much can be found in the literature on the morphology of the cell struts or membranelike windows of these foams. Wilkes et al. carried out a brief study of the morphology of a series of foams including high resilience foams with small angle X-ray scattering (SAXS) and DSC.[5] Some of the more conventional foams did not show a "Bragg peak" (evidence of phase separation) until the polyol was replaced with a polyol containing twenty weight percent polyurea grafts. The 3500 MW, trifunctional, secondary hydroxyl terminated polyols used in the conventional foams were replaced with a 6000 MW, trifunctional, primary hydroxyl terminated polyol in the high resilient foam. Also a lower water level and weaker surfactant were used. These foams showed a Bragg peak corresponding to spacings in the range of 5–20 nm. DSC showed that PEO crystallization was not present, and it was concluded that the Bragg peak was the result of hard segment microphase separation. Qualitatively it could be stated that the higher polyol MW and the weaker surfactant in the high resilient foams did more to allow phase separation to occur in this system than the presence of primary hydroxyls did to prevent it. This brief study, while not in depth, did illustrate that microphase formation could occur in foams. A new observation in view of structure–property considerations of these complex materials.

In summary, foam manufacture takes place in less than 5 min though foam properties will not stabilize until after 2 or more days of curing. The exothermic foam forming process involves competing blowing and gelling reactions. The foam mix is not homogeneous, and the precipitation of urea may somehow lead to or promote cell rupture. Evidence of urea precipitation also indicates that some type of phase-separated morphology exists in the foam and the existence of phase-separated domains of dimensions similar to those of segmented urethane elastomers has been observed in some foams using SAXS. Though polyurethane foams are in many ways similar to the extensively studied urethane elastomers, very little has been published on the morphology of the material comprising the cell structure. In this work, the results of a study on the morphology of a systematic series of foams with varied water content is presented. The effect of compression molding on morphology was also studied.

EXPERIMENTAL

Foam Preparation

The conventional slabstock foams used in this investigation were produced in a homemade, discontinuous box foam machine. The box foam machine consists of a mixing chamber and a 1 m^2 pasteboard box. The formulation components were combined in the mixing chamber using a procedure that mimicked the agitation process in a typical industrial foam machine. The

TABLE I
Description of Formulation Components

Polyol	Voranol 3100, a 3000 MW propylene oxide glycerine initiated polyether polyol from Dow Chemical
Isocyanate	T-80, an 80 : 20 mixture of the 2,4- and 2,6-isomers of toluene diisocyanate from Dow Chemical
Water/blowing agent	Deionized water, no blowing agent used
Catalysts	T-9, a tin catalyst from M & T Chemical (stannous octoate) DABCO 33LV, an amine catalyst from Air Products (33% DABCO or triethylenediamine in dipropylene glycol)
Surfactant	BF-2370, a silicone surfactant from Goldschmidt

mixed formulation components were immediately poured into the pasteboard box and allowed to react.

The formulation components used to produce these foams are summarized in Table 1. All components are commercial products that are used in the manufacture of conventional slabstock foams. A series of four foams was made in which the water content was varied from 2 to 5 parts per hundred parts polyol (pph) while maintaining the isocyanate index at 110. Catalysts and surfactant levels were held constant. Plaques were made by compression molding the foams at 204°C for 10 min.

The repeat units for the polyol (soft) and chain-extended (hard) segments are shown in Figure 1. The wt % hard segment and the average degree of chain extension for these four foams are presented in Table II. The calculations are based on complete reaction of the water and polyol active hydrogens and *do not consider* the 10% excess isocyanate. In light of the preceding discussion of foaming kinetics and the possibility of urea precipitation, it is emphasized that the calculated "average" chain extensions may not accurately depict the chain topology of the foams.

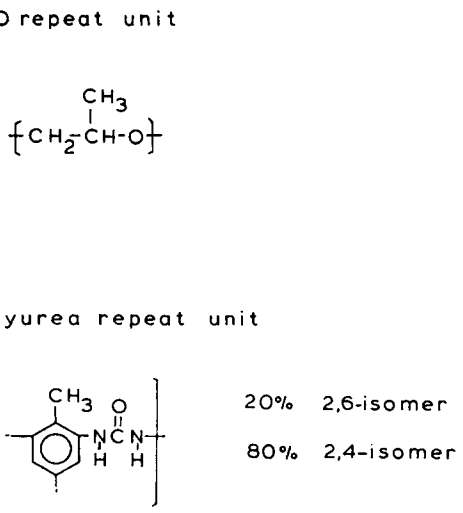

Fig. 1. Repeat units for PPO soft segment and a polyurea hard segment based on water extended TDI-80.

TABLE II
Composition of Foams[a]

Foam	Water (pph)	Hard segment (wt %)	Avg. end-to-end dist.[†] between crosslinks (nm)
1	2	21	3.2
2	3	26	4.3
3	4	30	5.4
4	5	34	6.5

[a] Calculations do not include the 10% stoichiometric excess of TDI.
[†] Based on bond lengths and use of Free rotation Assumption

Methods of Analysis

The structural and thermal properties of the foams and plaques were investigated using dynamic mechanical analysis, differential scanning calorimetry (DSC), swelling, transmission electron microscopy (TEM), scanning electron microscopy (SEM), wide angle X-ray scattering (WAXS), and small angle X-ray scattering (SAXS).

Dynamic Mechanical Spectroscopy (DMS)

Dynamic mechanical spectroscopy was used to locate the soft segment glass transition, observe modulus–temperature behavior, and to look for the presence of other thermal transitions. Experiments using the foams or plaques were performed using either a Rheometrics Model 605 mechanical spectrometer or a Rheometrics Model 7700 dynamic spectrometer. Foams were tested in a parallel plate mode using cylindrical samples as described elsewhere.[1] Foam samples were subjected to an oscillatory shear deformation at a frequency of 1 Hz and at a strain of approximately 1%. The temperature range was from −160 to 300°C. Data was collected at 5°C intervals. Temperatures were maintained for 2 min before readings were taken.

Differential Scanning Calorimetry (DSC)

DSC was performed on the foam series to determine the soft segment glass transition temperatures, to note the temperature stability of the foams, and to allow comparison of any other thermal transitions with dynamic mechanical data. The experiments were performed on a Mettler Model TA 3000. Samples were annealed in the DSC at 120°C for 5 min to drive off any absorbed moisture and then scanned from −120 to 250°C at the rate of 20°C/min.

Transmission Electron Microscopy (TEM)

The foams and plaques were investigated by transmission electron microscopy. A Joel 100C Analytical TEM was used and was operated at an accelerating voltage of 80 kV.

The foam samples were prepared by fitting small rectangles of foam into Beem capsules and imbedding the capsule with Dow epoxy resin DER 331 using a vacuum pump to remove entrapped air. The capsules were cured at 60°C for 8 h. The foams embedded in epoxy and the compression-molded

plaques were sliced into sections approximately 120 nm thick using a Sorvall MT-2 ultramicrotome at −80°C. Sections were placed on 300 mesh copper grids for the TEM analysis.

Scanning Electron Microscopy (SEM)

The plaques were immersed in liquid nitrogen (bp −196°C) for 5 min and then fractured. Suitable thickness slabs of foam were simply carefully "sliced" from a large foam sample at room temperature. Both types of samples were mounted on aluminum stubs and coated with 15 nm of Au/Pt using a SPI Model 13131 sputter. The Au/Pt was applied 5 nm at a time to avoid overheating the surface. Micrographs were taken on an ISI Super III-A scanning electron microscope operated in the secondary electron mode at a 15 kV accelerating voltage.

Wide Angle X-Ray Scattering (WAXS)

WAXS patterns were obtained for the foams and plaques to note the presence of possible crystalline or paracrystalline ordering and to note changes in structure due to the compression molding process. The WAXS patterns were taken in a standard Statton camera under vacuum and at a sample-to-film distance of 8 cm. The X-ray source was a Philips table-top X-ray generator PW 1720 equipped with a fine focus tube. The radiation was nickel-filtered CuKα with a wavelength of 0.154 nm. The plaques were approximately 1 mm thick. Foam samples were cut approximately 10 mm thick and compressed to less than 2 mm for the WAXS runs. Exposure times were 10–20 h depending on sample thickness, foam density, and hard segment content.

Small Angle X-Ray Scattering (SAXS)

Data were collected for the foams and plaques using the ORNL 10-m SAXS camera. This instrument features a rotating anode X-ray source, crystal monochromatization of the incident beam, pinhole collimation, and a 2-dimensional position-sensitive detector.[16] A copper anode was used, and the incident beam was monochromized to CuKα radiation. Details regarding data collection with the ORNL 10-m SAXS camera are given in Ref. 17.

Samples were prepared as in the WAXS experiments. The compression-molded plaques were used "as molded' at thickness of about 1 mm. Foam samples approximately 10 mm thick were compressed along the blow direction to about 6 mm for these experiments.

RESULTS AND DISCUSSION

Thermal Characterization

The temperature behavior of the foams and plaques was investigated using dynamic mechanical spectroscopy (DMS) and differential scanning calorimetry (DSC). The results of the DMS study were reported earlier by Spell et al.[1] Very briefly, the DMS spectra (G' and $\tan\delta$), for the foams are similar to those for relatively soft ideal elastomers (see Figs. 2 and 3). The storage

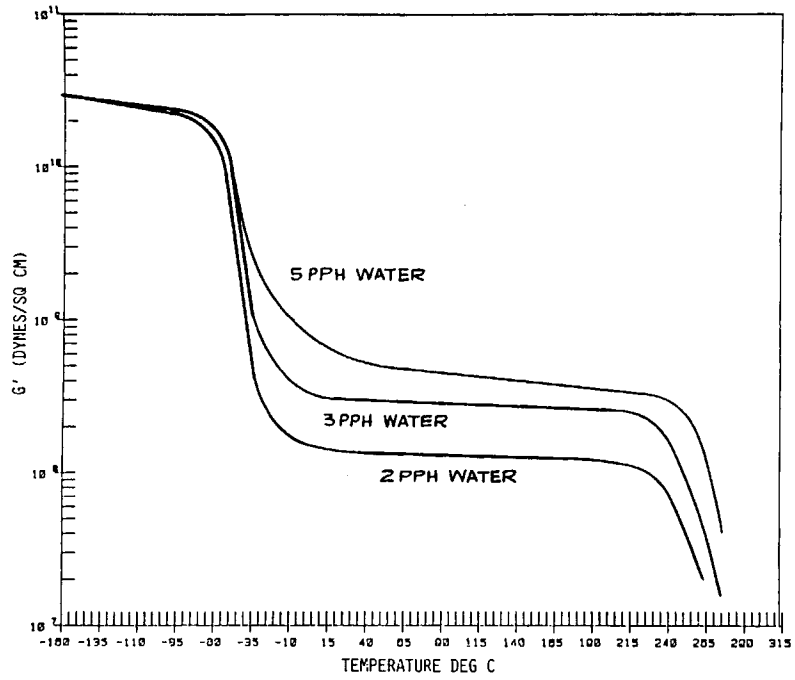

Fig. 2. Storage modulus G' for foams 1, 2, and 4 normalized at $-160°C$ to the level of polymeric glass (Ref. 1). Data for foam 3 not shown.

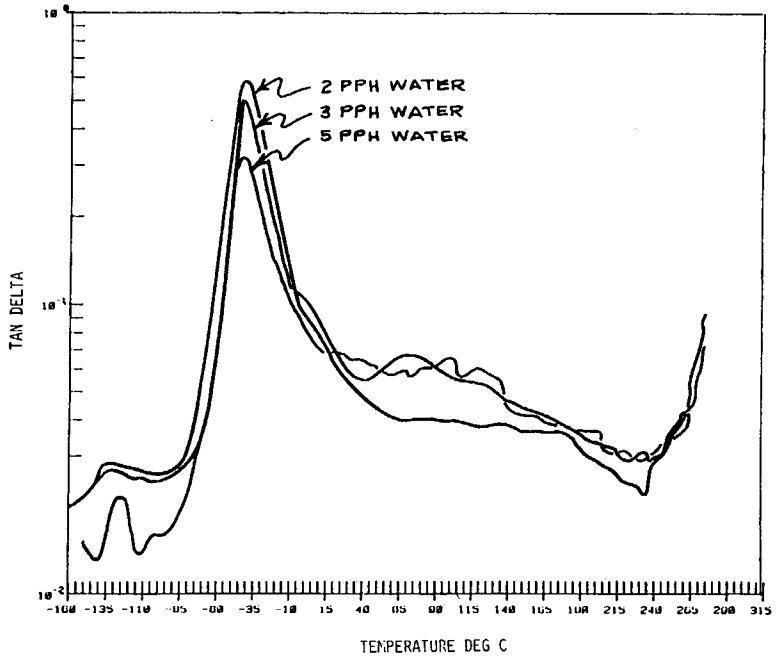

Fig. 3. Tan δ for foams 1, 2, and 4 (Ref. 1). Data for foam 3 not shown.

modulus curves each reveal a sharp transition from the glassy state to the rubbery state followed by a very extended rubbery plateau that exceeds 200°C after which degradation begins. The loss modulus curves in three of the four foams reveal a small and unexpected transition around 100°C (data not shown). When the spectrum is rerun immediately after passing through the transition and without exposing the sample to the atmosphere, the transition does not occur, and the modulus is slightly higher. The modulus also increases after thermal treatment in a nitrogen atmosphere. The small loss transition and modulus change is believed due to the loss of adsorbed moisture.

Comparison of the DMS tan δ spectra of the foams and plaques (data for plaques not shown) indicated that the compression molding process only slightly decreases the soft segment T_g, flattens the rubbery plateau, and extends the plateau to a slightly higher temperature. Only a small change in soft segment T_g suggests that the phase separation is only somewhat enhanced by the compression molding process. The somewhat extended rubbery plateau following molding may be caused by improved hard segment ordering (see later discussion).

Increasing the water content, which also increases the TDI content, interestingly, *does not greatly affect* the soft segment T_g. As might be expected, it apparently increases the high temperature stability, and increases the modulus as evidenced in the DMS spectra normalized to the glassy state (2×10^9 Pa). The results are summarized in Table III. The lack of change in soft segment T_g is clear evidence that a similar degree of phase separation between urea and polyol components exists in all samples.

To the author's knowledge, there are no other DMS studies of flexible polyurethane foams in the literature. This technique, however, has been commonly used to characterize the linear and crosslinked urethane elastomers.[18-21] In these latter systems, the soft segment T_g is often observed to decrease with increased soft segment molecular weight and increase with increased hard segment content as is explained on the bases of differing levels of phase separation. In addition the sharpness of the soft segment glass transition as well as the rubbery plateau becomes less distinct as phase mixing occurs. In comparison, the foams have superior elastomeric properties as evidenced by a sharp glass transition, well-defined rubbery modulii that are nearly independent of temperature (flat rubbery plateau), and have thermal stability to well above 200°C.

TABLE III
Thermal Transitions of the Series of Foams Studied

Foam	T_g (°C) by DMS[a]	T_g (°C) by DSC	T(hard) (°C) by DMS[c]
1	−40 (−43)[b]	−44.3	235
2	−38 (−40)	−46.4	245
3	−38 (−42)	−47.3	243
4	−41 (−42)	−47.9	250

[a] Values in parentheses are for the compression molded plaques.
[b] T_g is based on peak in tan δ.
[c] T(hard) is the apparent hard segment softening temperature.

To help account for our DMS results, the DSC studies of Sung and co-workers are pertinent. They determined the soft segment Tg of segmented elastomers with compositions having some similarity to polyurethane foams.[22] These elastomers were polyurethane–ureas and consisted of a linear PTMO soft segment and a 2,4-TDI–ethylenediamine hard segment. The soft segment T_g's were found to be lower than in PTMO/MDI-BD elastomers[23] and independent of hard segment content for a PTMO MW of 2000, indicating that phase separation improved when urethane linkages were replaced by urea linkages. In addition, Tyagi recently used the technique of DMS to characterize linear segmented MDI- and TDI-based polyurethane–ureas.[24] These polymers had PTMO soft segments and urethane–urea hard segments, the latter of which are somewhat analogous to those in water-blown polyurethane foams (i.e., hard segments of just the urea-linked aromatic isocyanate structures—no aliphatic character). In the MDI systems with a soft segment based on 2000 MW PTMO diols, the soft segment T_g was found to be about 25°C lower than in an analogous BD-extended systems and was also independent of hard segment content. With a TDI-based hard segment, the T_g was depressed further. Decreasing the soft segment molecular weight increased the soft segment T_g. The influence of hard segment concentration at lower MW was not determined. The rubbery plateaus for these linear urethane–ureas were also quite flat and extended above 200°C. Both the work of Tyagi[24] and Sung[22] shows that urea linkages lead to a higher degree of phase separation and promote higher temperature stability than urethane linkages. They also concluded that in elastomers with urea linked hard segments, the soft segment T_g is considerably less dependent on hard segment content as we have also found in this study.

The DMS results for the foams and their interpretation relative to those for the TDI-based polyurethane–urea elastomers are strikingly similar. This comparison indicates that, despite the possibilities for a much more complex network morphology in the foams, their behavior is governed by the same forces that determine the DMS behavior in a system of linear segmented molecules synthesized under more controlled conditions.

Complimentary DSC data was collected for the foams (see Table III). The data shows glass transition values that are slightly lower than those from the DMS spectra and decreased slightly with increasing water content. The small difference in T_g values is due to the usual kinetic effects of T_g on rate of measurement. It may be noted that, on the first temperature scan of each foam, a broad low energy endotherm occurs over a temperature range of from 20 to 120°C, maximizing at about 80°C. If the samples are immediately rerun or if fresh samples are annealed at 120°C for 5 min and then run, the endotherm is not observed. This endotherm is again believed to be caused by the release of adsorbed moisture and to correspond with the energy loss transitions observed in the DMS study. No other peaks or transitions are observed before the onset of degradation. As in the DMS study, the onset of degradation begins at higher temperatures when the hard segment content is higher.

DSC studies were also carried out on the compression molded foams, and the results of the T_g analysis are also given in Table III. The slightly lower values suggest somewhat better phase separation of the soft segment material

which supports the DMS data discussed above. Note, however, that the differences are not large—a point to be utilized later.

Transmission Electron Microscopy (TEM)

Transmission electron micrographs for foams 1–4 are shown in Figures 4(a)–(d). The micrograph for foam 1, the foam with the lowest water content, has a diffuse grainy texture on the 100 nm level [Fig. 4(a)]. This diffuse grainy texture is not visible in the adjacent epoxy matrix, strongly indicating that this observed texture is real. The general weak contrast, and variation in grain sizes indicate that the contrast probably originates from features much smaller than the 120 nm thickness of the specimen. This observation agrees with the fact that the compression molded plaque of this foam is *transparent.* Again, these diffuse grains vary in size and contrast, and most importantly are randomly dispersed.

The micrograph for foam 2 is shown in Figure 4(b). The increase in hard segment content now results in improved contrast and the appearance of what are believed to be larger aggregations based principally on precipitated rich polyurea regions. In the micrograph there are large whitish-grey areas which are believed to result from regions of lower electron dense material, i.e., lower concentration of TDI. (Some of the grey bands result from variations in sample thickness.) It is the darker dense regions that are believed to be precipitated polyurea, and are roughly 100 nm in diameter and are randomly dispersed (meaning some are isolated and some are agglomerated into groups of ca. 300 nm). The hard segment dense regions are surrounded by lighter grey regions, giving the impression that the dispersion of the urea aggregates or "urea-rich regions" is semicontinuous, but this may be a consequence of film thickness and overlap of these darker regions.

The micrographs for foams 3 and 4 are shown in Figures 4(c) and 4(d) respectively. The size of the aggregate regions increases with water content—again in line with the increase in urea content. For foam 4 these regins are about 300 nm in diameter. This agrees with the observation that *opacity increases with water content in the corresponding plaques.* The presence of random agglomerations and the semicontinuous nature of the aggregates are somewhat similar to that observed in foam 2. Micrographs for compression-molded plaques 3 and 4 are not shown here, but were very similar to those of foams 3 and 4, respectively.

As pointed out earlier, Rossmy et al.[9,10] studied the sequence of reactions in foam making with IR spectroscopy. When the reacting foam mix reached about 80°C, the urea carbonyl absorption shifted and the clear foam mix turned opaque. Through IR studies on model compounds it was concluded that the shift in carbonyl absorption was the result of the precipitation of a macroscopic urea phase.

With the earlier remarks regarding urea precipitation, the formation of urea aggregates into a larger macrostructure in the foams as observed by TEM cannot be viewed as a surprise.

Scanning Electron Microscopy (SEM)

The use of scanning electron microscopy (SEM) at low magnifications, provided information on the relative cellular textures of the four foams (see

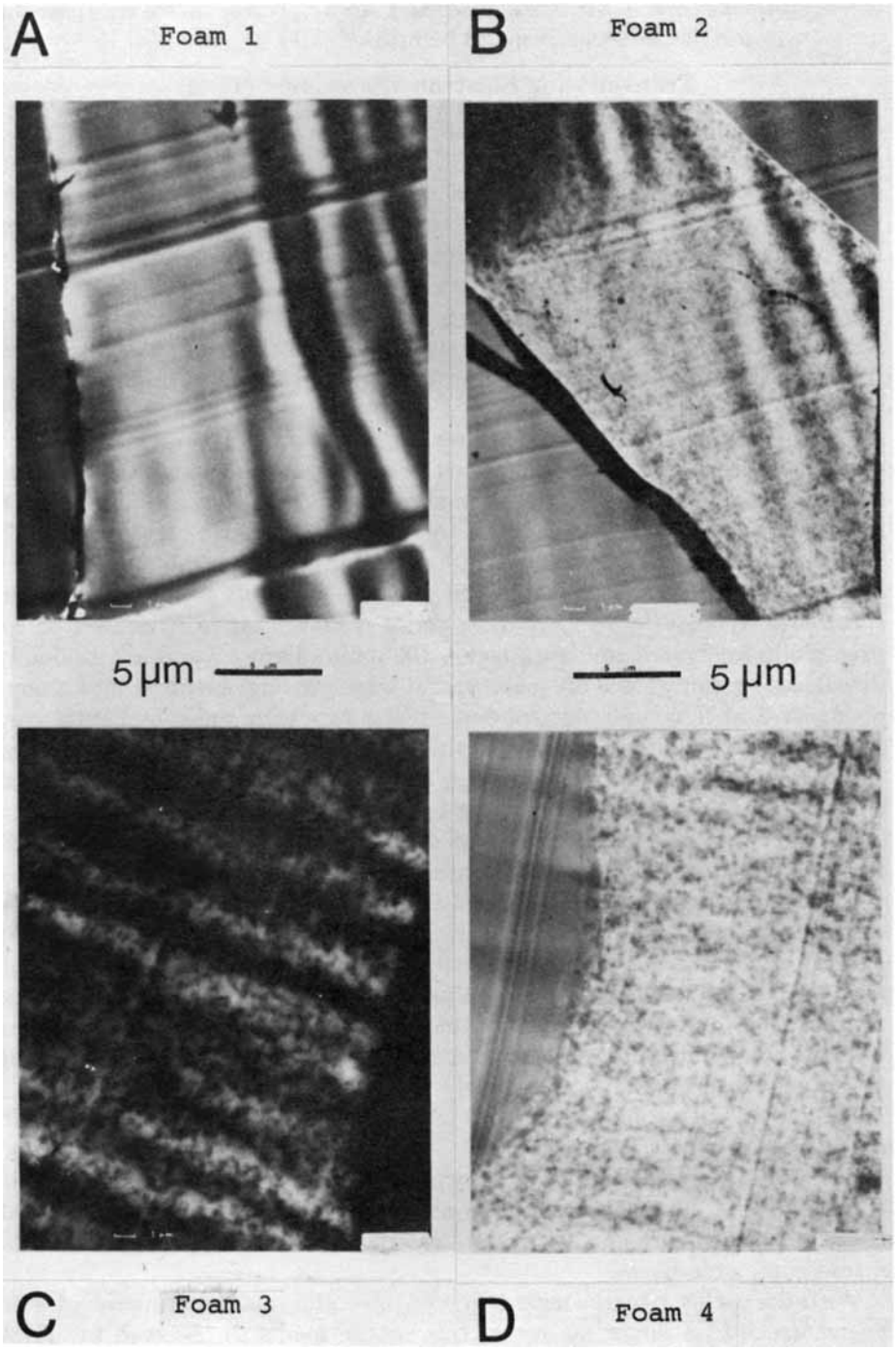

Fig. 4. TEM micrographs for foams 1–4.

Figs. 5 and 6). It is noted from these figures that, for a given foam, the two different views of the material clearly display an inherent structural anisotropy when observed orthogonal to the blow axis direction. However, when any of the foam structures are observed parallel to the blow axis, cylindrical symmetry exists as expected. For this reason, all SAXS experiments (described earlier in this paper) were carried out with the incident beam parallel to the blow axis.

At higher magnification, scanning electron microscopy also provided additional evidence for a multiphase phase morphology with randomly dispersed agglomerations 100–300 nm in size [see Figs. 7(a)–(d)]. Cold fracture surfaces

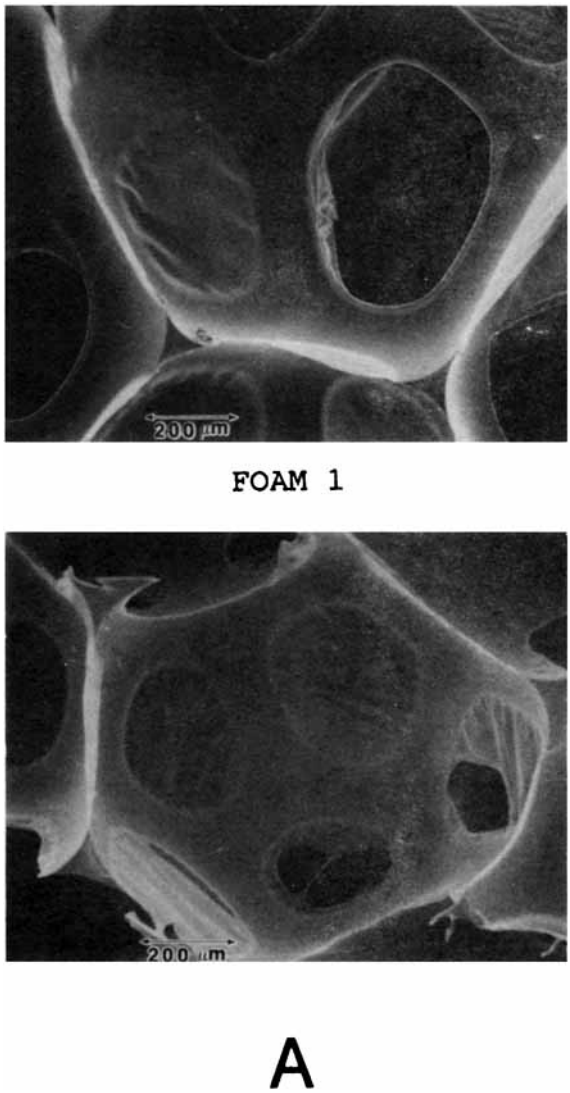

Fig. 5. SEM micrographs of foams 1 and 2: (A) Observation direction parallel to the blow axis; (B) observation direction perpendicular to the blow axis.

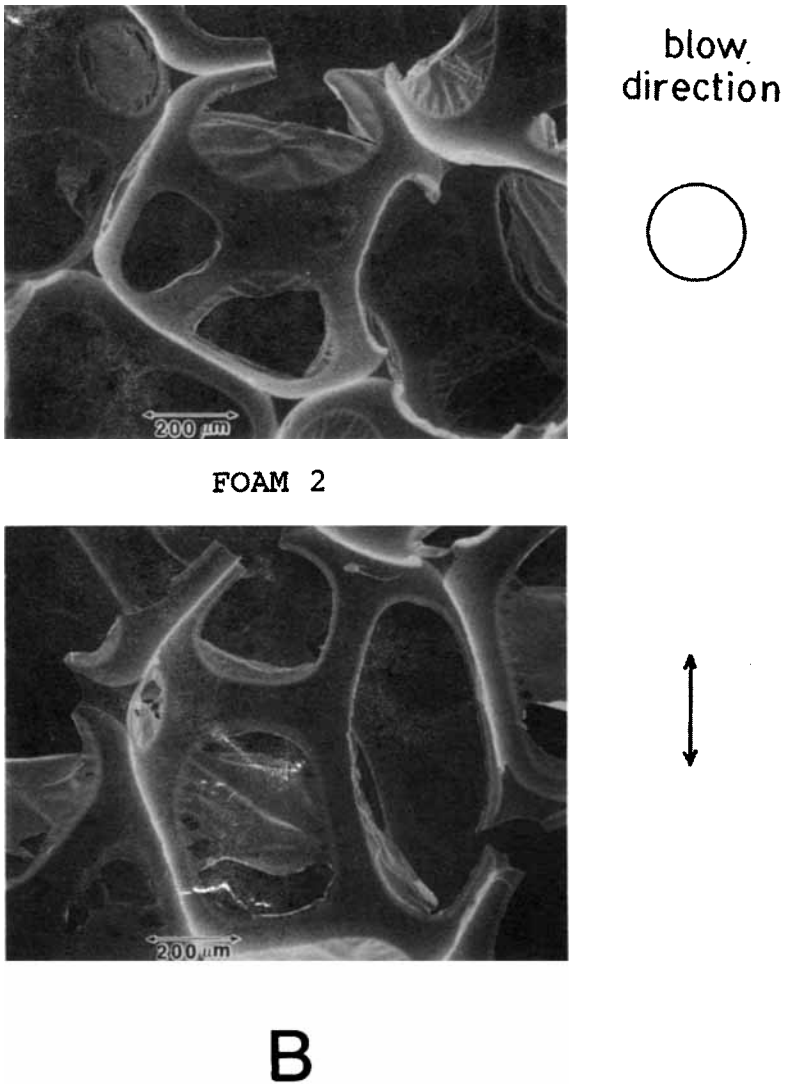

Fig. 5. (*Continued from the previous page.*)

of plaques 1–4 were studied. The fracture surface of plaque 1 is smooth, agreeing with the TEM micrograph of foam 1, which depicts no observable microstructure on the 100 nm level. The SEM micrographs for plaques 2, 3, and 4 show increasing surface texture with increasing TDI/water content. In plaques 3 and 4 discrete 100–300 nm protuberences are visible. The random distribution of the protuberences and, at times, the random continuity between them are very much like that observed by TEM.

Wide Angle X-Ray Scattering (WAXS)

Wide angle diffraction patterns for foams 1–4 are shown in Figure 8. All of the foam show a diffuse halo and what appears to be an apparent diffraction

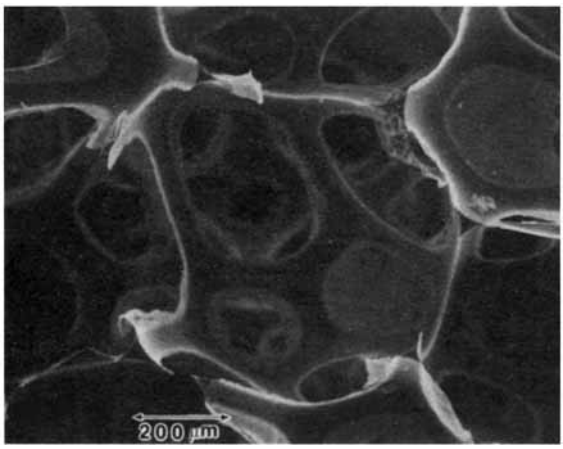

FOAM 3

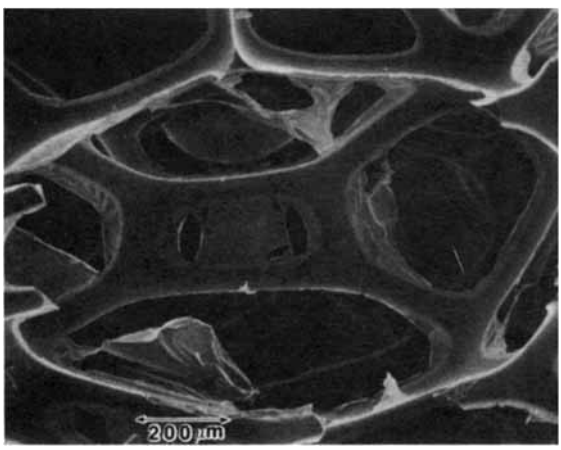

A

Fig. 6. SEM micrographs of foams 3 and 4: (A) Observation direction parallel to the blow axis; (B) observation direction perpendicular to the blow axis.

peak corresponding to 0.45 nm. Foams 2–4 have a second weaker peak at 0.59 nm. Interestingly, the peaks sharpen with increased hard segment content and are clearly too distinct to arise from maxima of the amorphous halos.

The WAXS patterns for the compression-molded plaques resembled those of the respective foams again implying that the compression molding operation *did not greatly change the morphology as viewed by this method.* A brief annealing study was carried out in an attempt to sharpen the diffraction peaks. Foam 4 was annealed for 16 h at 200°C. The WAXS pattern did not reveal significant changes. However, WAXS patterns for plaque 4 *before and after DMF swelling* are shown in Figures 9(a) and (b). The plaque that was

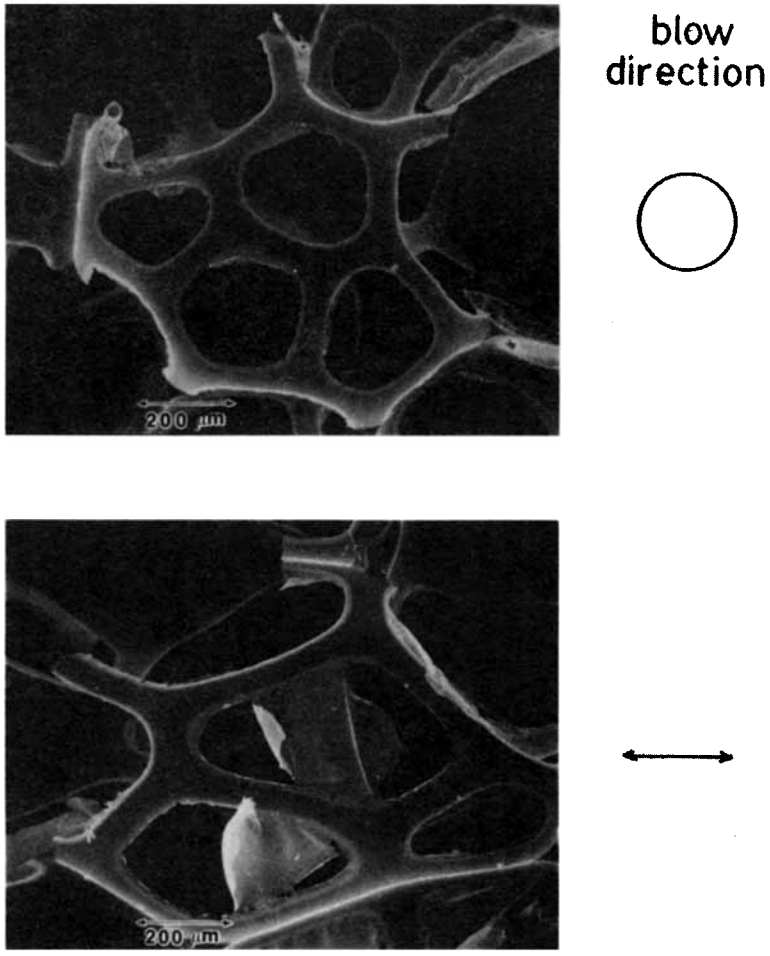

Fig. 6. (*Continued from the previous page.*)

exposed to the solvent does not have the 0.59 nm maximum, and the peak at 0.45 nm is more diffuse than it was before swelling. The untreated plaque also showed a diffuse halo centered about 1.6 nm. This latter halo had not been well observed in the other foams or plaques—possibly because they had somewhat shorter exposure times.

Several workers have used WAXS to study polyurethane–ureas with noncrystalline hard segments.[22,25,26] Both Chang and Wilkes[25] and Sung et al.[22] showed that the hard segment was responsible for an amorphous halo with a maximum in the 0.4–0.5 nm range. Recently, a TDI-80/20-based water-extended polyurea synthesized in this laboratory[24] had a broad

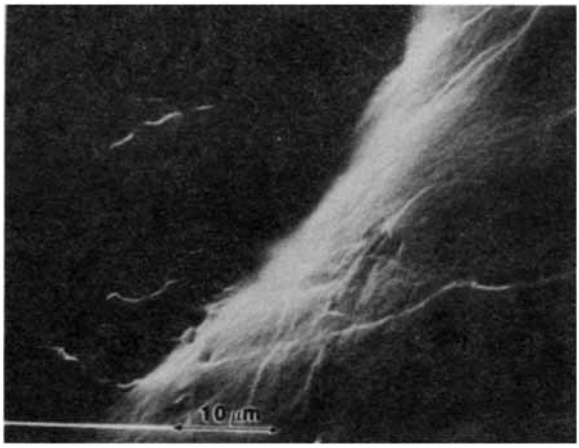

A - PLAQUE 1

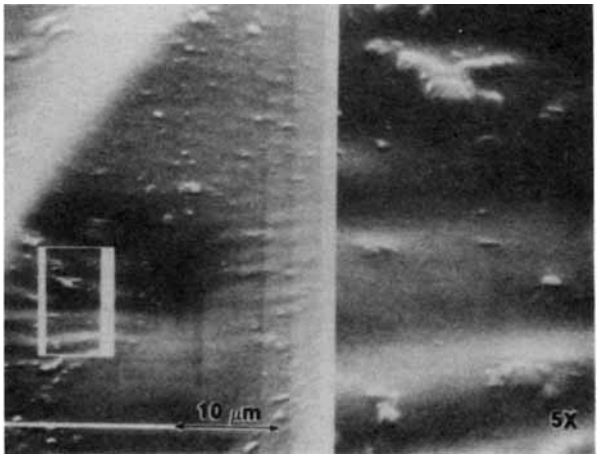

B - PLAQUE 2

Fig. 7. SEM micrographs of cold fracture surfaces of plaques 1–4.

amorphous halo in the 0.4–0.6 nm range and a narrow diffuse halo centered about 1.6 nm.

Based on the above studies, we believe that the amorphous halo in all the foams and plaques can be attributed to randomness associated with hard and soft segments. However, the 0.45 and 0.59 nm peaks are taken as an indicator of increased order of the hard TDI segments, even though the TDI material is a 80/20 mixture of the 2,4- and 2,6-isomers. The origin of these peaks is unknown but is probably a result of some paracrystalline ordering of the hard segments through hydrogen bonding. Similar peaks are observed in MDI–BD urethanes and also have been attributed to paracrystalline order,[27] where this

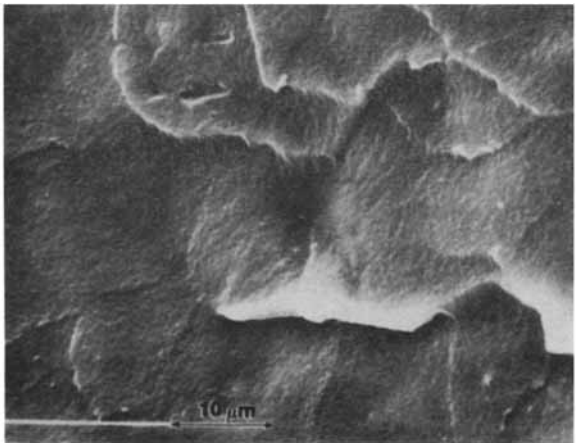

C- PLAQUE 3

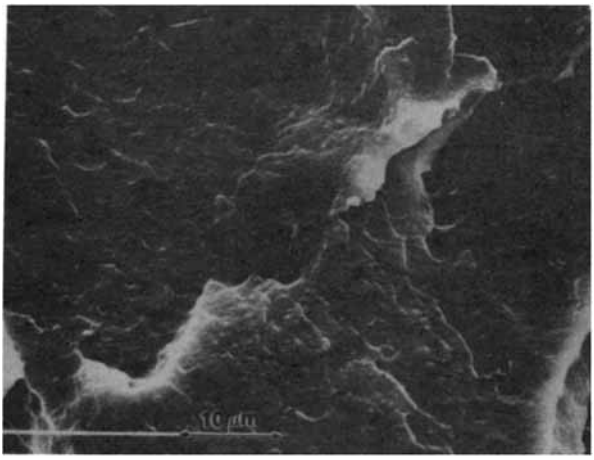

D- PLAQUE 4

Fig. 7. *(Continued from the previous page.)*

ordering is not a minimum free energy state but results from the formation of a stable hydrogen bonding network. The surprising feature is that this higher level of ordering was unexpected based on the isomer mixture of 2,4- and 2,6-TDI.

The WAXS patterns did not change noticeably as a result of compression molding indicating that this thermal process does not have a major effect on hard segment ordering. The swelling in DMF and subsequent drying of plaque 4, however, resulted in a decrease in hard segment order. One explanation for this is that the extraction process removed a portion of the paracrystalline

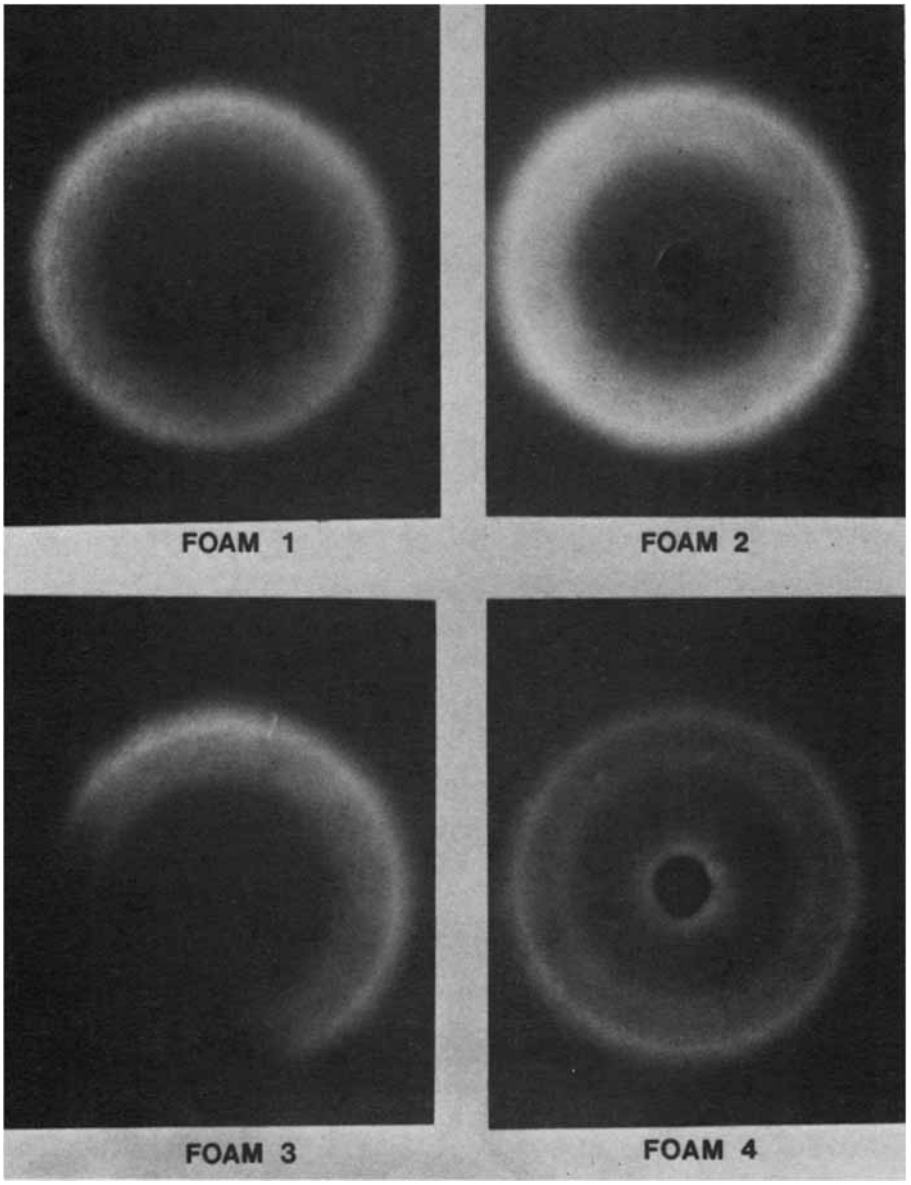

Fig. 8. WAXS patterns for foams 1–4 showing evidence of increased order with higher hard segment content.

polyurea phase. A second more likely explanation is that the presence of the solvent disrupted the hydrogen bonding network that was formed during foam rise and cure. The diffuse ring observed at 1.6 nm in the untreated plaque 4 probably arises from the hard segment. A diffuse ring was observed for the polyurea at the same spacing. Spacings of this magnitude have been observed in MDI–BD urethanes and were associated with the length of hard segment repeat unit.

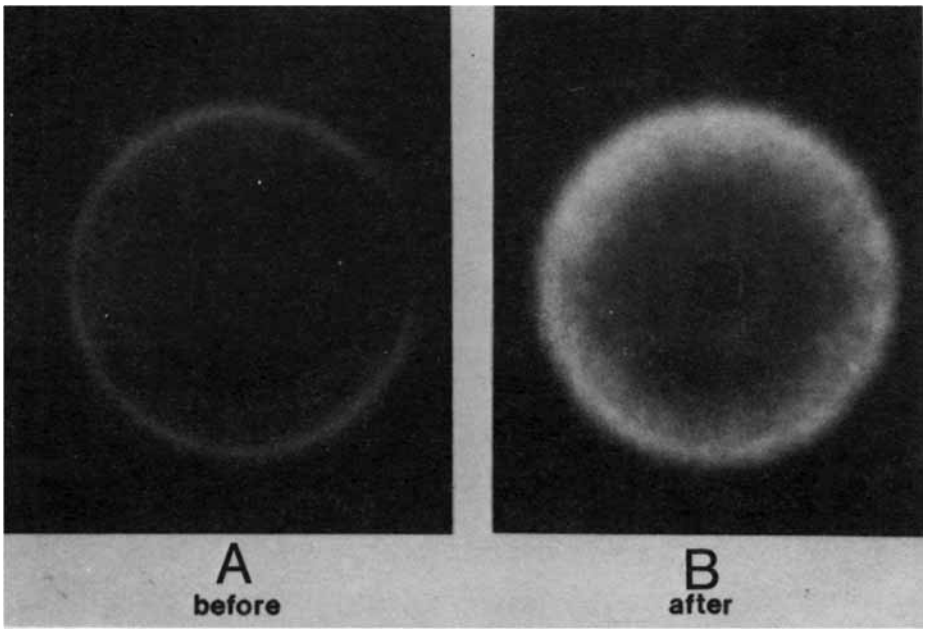

Fig. 9. WAXS patterns for plaque 4 *before* and *after* extraction with DMF.

SAXS Analysis

Figures 10 and 11 show the scattering profiles for plaques 1–4 and foams 1–4, respectively, as a function of the scattering vector κ. These curves are comprised of data collected at 1- and 2-m sample-to-detector distances. They show corrected relative intensities, and are the result of the standard data treatment (background subtraction, zero angle extrapolation, tailfitting, smoothing). Several comments can be made about the foams and plaques just from the shapes of the scattering profiles. First, all of the scattering curves have a shoulder, and the shoulder appears in approximately the same position for all the foams or plaques of the series. Each of these shoulders can be thought of as an interference or correlation peak that is not completely resolved due to occurring at low scattering angles and being quite diffuse. The 2–100 nm morphological features that give rise to SAXS are typically not expected to be of the same size, shape, or separated by the same distances. As a result, sharp peaks are generally not seen in SAXS although they can often be narrower than observed here. By applying Bragg's law to the shoulders in Figure 10 and 11 an *estimate* of the center-to-center (interdomain) distance between scattering particles is obtained. This distance for the plaques is approximately 10 nm and increases only slightly with increasing water content. This same periodicity for the foams is only about 10% smaller at 9 nm and again increases with water content. These results are summarized in Table IV. The reader should not confuse this estimated interdomain distance with the polyurea aggregates discussed earlier as were observed with TEM and indirectly via SEM.

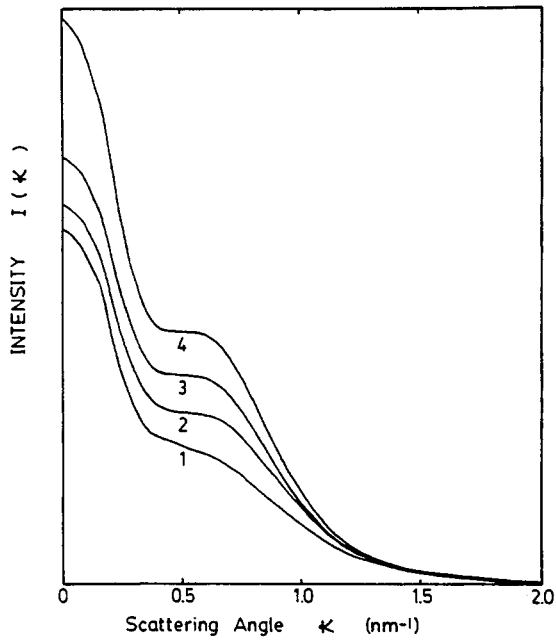

Fig. 10. Scattering profiles for plaques 1–4. Scattering are the result of extrapolation to zero angle, background removal, tail fitting, and smoothing and show correct relative intensity. $\kappa = (4\pi/\lambda)(\sin\theta/2)$, where θ is the radial scattering angle.

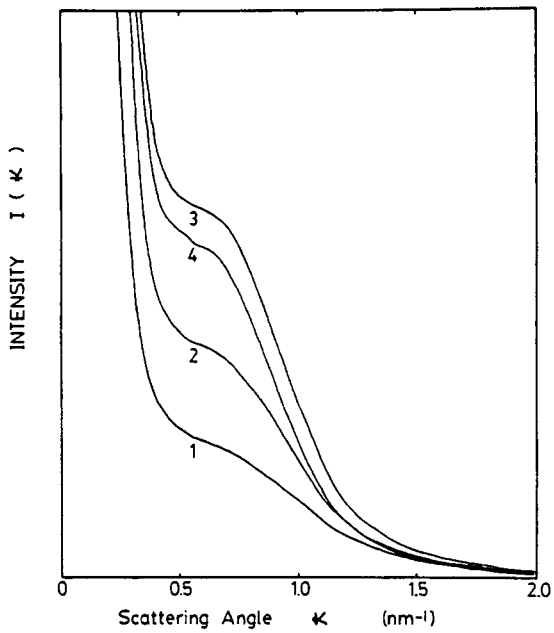

Fig. 11. Scattering profiles for foams 1–4. Scattering are the result of extrapolation to zero angle, background removal, tail fitting, and smoothing and show correct relative intensity. $\kappa = (4\pi/\lambda)(\sin\theta/2)$, where θ is the radial scattering angle.

TABLE IV
Interparticle Spacing (nm)

	d	R	X
		Foam	
1	8.9	6.9	6.6
2	9.4	7.3	6.7
3	9.4	7.7	6.9
4	9.6	7.2	7.1
		Plaque	
1	10.0	9.0	6.9
2	9.9	9.1	7.0
3	10.2	9.5	7.3
4	10.6	9.6	7.4

[a] d = Bragg's law; R = 3-D correlation function, first maximim; X = 1-D correlation function, first maximum.

A second comment on the scattering profiles in Figures 10 and 11 is that the measured intensity increases with increasing water content. This is indeed expected given that the contrast factor for small angle scattering from an ideal two-phase system with sharp phase boundaries is given by

$$\overline{\Delta\rho}^2 = \phi(1)\phi(2)[\rho(1) - \rho(2)]^2 \quad (1)$$

In the above expression, the contrast factor $\overline{\Delta\rho^2}$ is called the mean-square electron density variance, $\phi(1)$ and $\phi(2)$ are the electron densities of phases 1 and 2, and $\phi(1)$ and $\phi(2)$ are volume fractions. For a given system $\rho(1)$ and $\rho(2)$ are constant and the volume fractions determine the amount of contrast. Since $\phi(1)$ and $\phi(2)$ must sum to 1, the contrast reaches a maximum for a 50–50 mixture of phases [at constant $\rho(1)$ and $\rho(2)$]. It is recalled that, within our systems, the hard segment content never exceeds 34%. Also note that the contrast is independent of which phase has the higher electron density. In Figure 10, the intensity increases as hard segment content of the plaques increases. In Figure 11, the expected behavior is observed except for foam 3 where the intensity is somewhat greater than foam 4. One explanation for the transposition of foams 3 and 4 is that the measured intensity is improperly normalized by dividing by the thickness (corrected with bulk density) of the foam. The normalization may not be sufficient if the X-ray beam does not traverse a statistically sufficient number of cells to insure that a representative proportion of windows, voids, and struts is always seen by the beam. As a result, there is a degree of uncertainty in knowing how much material was actually exposed to the X-ray beam.

A final observation that should be addressed is the difference in low angle scattering between the foams and the plaques. In particular, the plaques displayed a near zero angle intensity that is nearly two to three times the shoulder intensity. In contrast, the foams show a near zero angle intensity that is about 8–15 times their respective shoulder intensity. This increased intensity at very low angles is strongly believed to arise from both surface

reflections and Bragg Law interferences due to the presence of small voids (cell structure) and is not believed due to domain morphology within the struts of the foam. Indeed, such reflection behavior and influence of the large cell voids adversely effects the SAXS analysis associated with curve fitting this portion of the scattering profile or integration of the scattering profile. It is believed that the higher intensity very low angle scattering should not, however, strongly influence the position of the shoulder or interference peaks caused by the domains or the analysis concerned with the tail region of the scattering profile. Some support for this latter statement can be given in that the plaques and the foams showed shoulder positions of nearly the same value although the foams provided a somewhat smaller angle shoulder accordingly which lead to a difference of about 1 nm larger estimated interdomain spacing. It would seem that if this extra low angle scattering were dominant with respect to influencing the interdomain interference, this near similarity between foams and plaques would not have occurred. With this in mind, and the fact that likely some error is introduced by the presence of "extra" small angle scattering of the foams, some additional analysis of the SAXS results will be provided through a correlation function analysis.

Correlation Function Analysis

The well-known correlation function $\gamma(r)$ as derived from analysis of the SAXS behavior for a given sample provides the probability that a rod of length r will have both ends in regions of the same electron density. It is calculated by integrating the scattering profile for contributions due to scattering centers a distance r apart and then dividing by the integrated intensity for all possible correlations.[28] Because the correlation function is a ratio of two integrals, the influence of the increased low angle intensity in the foam data may be at least partially normalized out. However, if the increased low angle scatter does influence the correlation function, it would shift the correlation probability to larger values. The first maximum in a 3-dimensional correlation function should relate to the interparticle spacing, which so far has been approximated by applying Bragg's law to the "shoulder" in the scattered intensity. The first maximum in a 1-dimensional correlation function gives the average distance between scattering centers when a lamellar morphology is assumed.

Both correlation functions were calculated for the foams and plaques. The results are listed along with the Bragg's law spacings in Table IV. The positions of the first maxima in the 3-dimensional correlational function is somewhat less than the Bragg's law spacing for both the foams and plaques. This decreased value is, in fact, generally observed [24,29] and arises from the relative weighting of different size particles by the two methods. The first maximum of the 3-dimensional correlation function is thought to be the better estimate of center-to-center particle spacing. A plot of the correlation function for plaque 3 is shown in Figure 12. The 3-D correlation function shows a weak maximum at 9.5 nm. The breadth of this peak again strongly suggests a distribution of interdomain spacings. The 1-D correlation function has a much sharper maximum located at 7.3 nm. Neither correlation function shows repeated maxima, thereby indicating a lack of long range order.

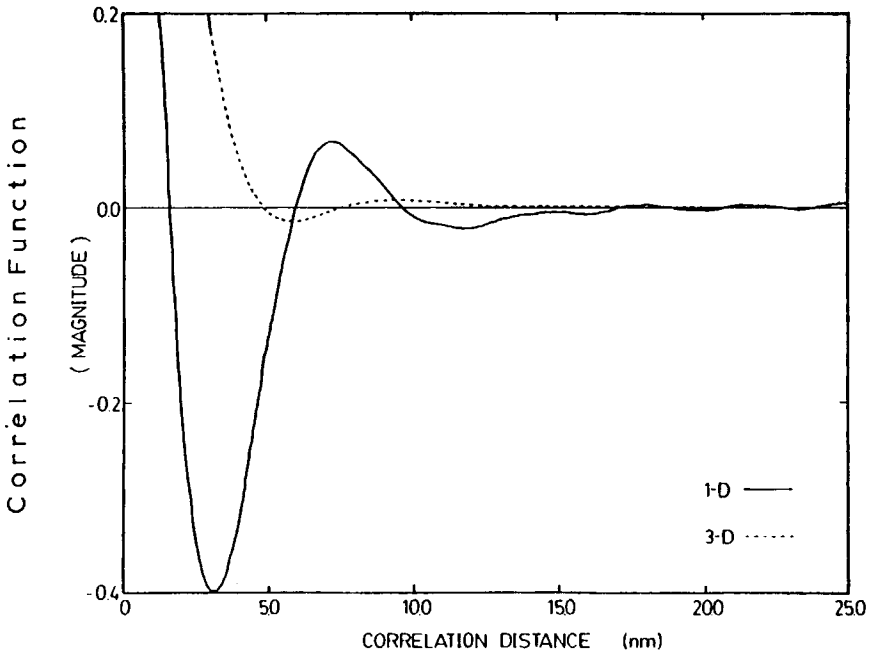

Fig. 12. One-dimensional and three-dimensional correlation functions for plaque 3.

The correlation distances for the foams are again somewhat smaller than for the plaques (particularly when obtained by the 3-dimensional correlation function), indicating that the increased low angle scatter in the foams did not appreciably affect the correlation function calculations (recall the earlier discussion). The 3-D and 1-D correlation functions for foam 3 are shown in Figure 13. The 3-D correlation function has a maximum at 7.7 nm. This lower maximum may be the result of the correlation function not dropping below zero before the maximum. Comparison of the 3-D correlation functions for the foam and plaques suggests a more continuous distribution of hard segments in the foams. The 1-D correlation function has a maximum at 6.9 nm. As with the plaques, there is little periodicity in the correlation functions of the foams, suggesting a lack of long range order as expected.

The correlation functions for the other plaques and foams closely resemble Figures 12 and 13, respectively. The correlation distances generally increase slightly with hard segment content, possibly suggesting the presence of slightly larger domains. The slightly smaller correlation distances of the foams as compared to the plaques is believed real, but there is some slight possibility that this difference could be the result of the orientation of the domains in the compressed foam in the beam. Specifically, the domains may be elongated in the blow or rise direction of the foam and thus would appear smaller when observed looking down the blow axis which was utilized in all SAXS experiments on foams 1–4. In the plaques, however, these domains would be more randomly oriented and on the average appear larger. It might also be stated that the larger correlation distances in the plaques could also result from improved phase separation and the formation of somewhat larger domains

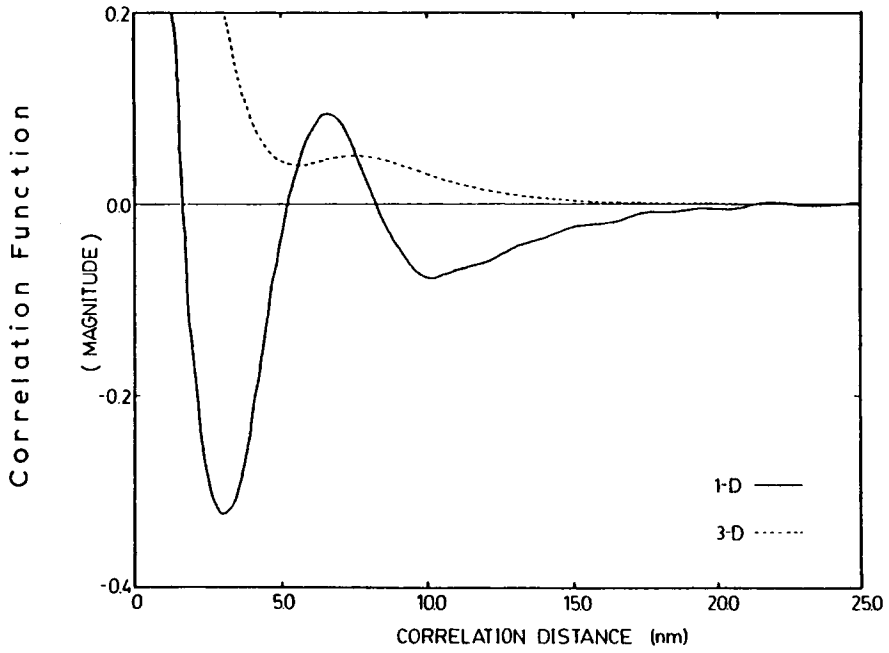

Fig. 13. One-dimensional and three-dimensional correlation functions for foam 3.

during the compression molding process. This latter speculation would be in line with the conclusions based on the DSC and DMS results in that the plaques tend to display a slightly enhanced phase separation of the polyol soft segment material.

As a point of contrast, in TDI based linear segmented urethane or urethane–urea elastomers, observed SAXS periodicities 20–50% higher than those reported here have been observed.[29,30] These systems, however, were chain extended by ethylene glycol or ethylene diamine and made with linear polyols. The shorter, stiffer hard segments in the foams and the use of trifunctional polyols both would act to hinder the formation of large domains as compared to these elastomers. The smaller d-spacings in the foams are, on this basis, very reasonable.

Interfacial Boundary Thickness between Hard and Soft Segment Regions

According to Porod's law, the scattered intensity for a two-phase system with sharp phase boundaries provides in the limit of high scattering angles (the tail region) the relationship given as

$$I(\kappa) \sim K_p/\kappa^4 \tag{2}$$

where κ is a function of the scattering angle and K_p is a constant related to the area of interface per unit volume.[24-26] In the limit of high scattering angles, the product $K^4 \cdot I(\kappa)$ should be constant. When this product increases with increasing scattering angle, the material is said to show positive devia-

tion from Porod's law. Positive deviations can result from thermal fluctuations (background intensity) and from the isolation of either a soft or hard segment in the wrong phase (phase mixing). Negative deviations result from the diffuse boundary or gradient in electron density between phases.

To characterize the diffuse boundary, the scattering contribution for background intensity must be subtracted and the scattering for phase mixing must be assumed negligible. This assumption may not be valid as suggested by a Porod analysis of a series of foams of constant water content and increasing TDI index. While not discussed within this paper, we have noted that, as the TDI index increased, positive deviations from Porod's law are systematically observed thereby indicating an increased phase mixing. However, at a constant index level, *as in this study,* the degree of phase mixing is not known, but, if it is assumed constant, then at least relative values of the diffuse boundary thickness can be calculated which provides additional information on the variation in morphological details.

The diffuse boundary thicknesses were determined assuming a sigmodial gradient for the domain interface as has been quite well justified on the basis of theory.[34-36] The observed scattering data were fit to the product of a smoothing function and ideal Porod's law scatter as discussed elsewhere.[36] The index of interfacial thickness provided from this analysis is a parameter denoted as σ. This parameter represents the half-width of the diffuse boundary where the smoothing function has a value of 0.606 (see Fig. 14). The width of the diffuse boundary assuming a linear gradient in electron density across the interface is about 3.5 times sigma, i.e., $E = \sqrt{12}\,\sigma$.

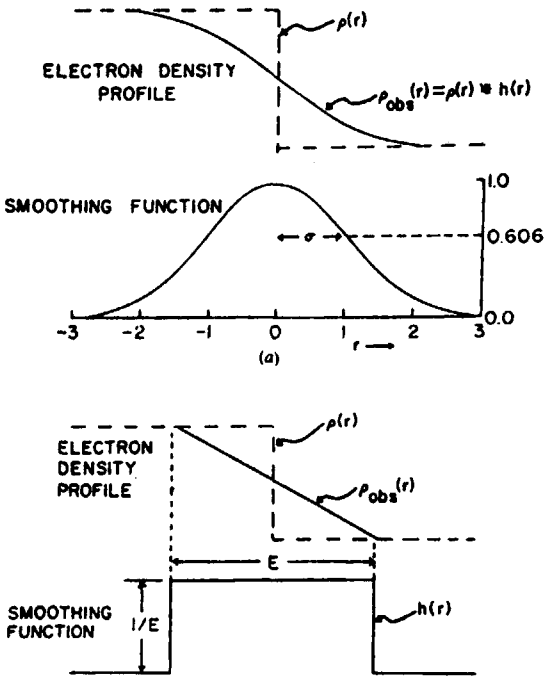

Fig. 14. Relationship of to the diffuse boundary thickness and comparison of sigmoidal gradient to a linear gradient (Ref. 30).

TABLE V
Diffuse Boundary Thickness (nm)[a]

	Sigma (1 m)	Sigma (1 and 2 m)
	Foam	
1	0.23	0.23
2	0.40	0.39
3	0.51	0.44
4	0.52	0.53
	Plaque	
1	0.30	0.27
2	0.43	0.42
3	0.53	0.49
4	0.57	0.53

The results of the Porod law analysis are summarized in Table V. For the foam series, foam 1 shows a σ value of 0.23 nm, and these values increase with hard segment up to 0.53 nm for foam 4. The reverse trend might be expected based on the formation of larger, better ordered domains with increasing hard segment content. The observed trend, however, indicates that the lengths of the chain extended hard segments are likely more polydisperse with increasing water content and that improved ordering (at the interface) may not be as possible with such asymmetric hard segments. The plaques have only slightly larger diffuse boundaries and show the same trend with increasing hard segment content. The reader again will note that the differences between plaques and foams are not greatly different. The slightly larger boundary thicknesses in the plaques point again toward somewhat larger domains in these materials, although this measurement does not confirm this speculation.

It should be pointed out that the sigma (σ) values reported here for the foams and plaques are of the same range as the values that have been commonly reported for TDI-based urethane and urethane/urea elastomers.[29,30,37] This again supports our view that while there are differences in morphological detail in the foams relative to the urethane or urethane–urea elastomers, there are also some similar features with regard to hard segment domain character in terms of similar interdomain correlation lengths and interface boundary thicknesses.

CONCLUDING REMARKS

In summary of the structural studies carried out on these somewhat conventional water blown TDI–PO–water blown foams, we suggest the general morphological structure to be somewhat as shown in Figure 15. Within this simplified morphological picture is shown a large scale structure that results from urea rich percipitants that we have termed aggregates within this paper. These structures have been noted through the use of microscopy techniques and are believed to likely result in any common urethane–urea-blown foam

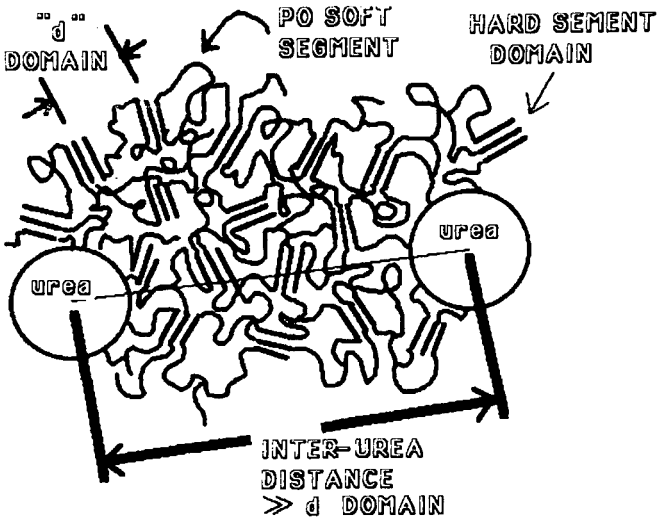

Fig. 15. Simplified schematic morphological model of the perceived foam textures—particularly those with significant TDI content which leads to greater urea precipitate formation. The "sticklike" hard segments are not necessarily as linear nor as uniform in length as the figure implies.

where sufficient urea-rich segments are formed early in the reaction which have limited solubility and promote this precipitation. These aggregates are believed to be of a reinforcing nature within the system and in fact may well help promote cell rupture of the window structures of the cells thereby leading to general strut formation—an essential feature of open cell foam structures. While no proof exists at this time, we would speculate that these urea aggregates are at least partially bound to the matrix material due to the potential of their surface diisocyanate or amine groups that could react with matrix polyol hydroxyls. Besides the formation of these aggregates, however, there is also the development of the more common microdomain or hard segment domain structure that should not be confused with the former aggregates. This latter structure is believed to be rather typical of what is also found in the urethane or urethane–urea elastomers as well documented over recent years. The size of these domains and their interfacial boundary thicknesses with the soft segment region are also believed to be rather comparable based on the evidence obtained through small angle X-ray analysis. While further work is certainly suggested for better verifying what we have proposed here in a simple morphological model of these urethane–urea foams, we believe this picture offers a good base upon which to develop a more refined understanding of the structure–property behavior of the solid state portion of these highly important materials.

The authors would like to thank Dr. J. S. Lin and the Oak Ridge National Laboratory for granting us beam time and assisting us in the utilization of the 10 m SAXS system.

References

1. R. B. Turner, H. L. Spell, and G. L. Wilkes, SPI 28th Annual Technical/Marketing Conference, 1984, p. 244.

2. V. P. Chebotarev, F. A. Kryuchkov, and O. G. Tarakova, *Plast. Massy.*, 53 (1969); *Sov. Plast.*, **8**, 50 (1969).
3. W. Patten, C. G. Seefried, and R. D. Whitman, *J. Cellular Plast.*, **10**(6), 276 (1974).
4. G. E. Corbett and B. V. Wadie, *J. Cellular Plast.*, **10**(1), 26 (1974).
5. G. L. Wilkes, S. Abouzahr, and D. Radovich, *J. Cellular Plast.*, **19**(4), 248 (1983).
6. G. Hauptmann, K. H. Dorner, H. Hocker, and G. Pfisterer, "Cellular and Non-cellular Polyurethanes," International Conference, Strassbourg, France, Urethane Division, SPI, 1980, p. 635.
7. F. E. Bailey, Jr. and F. E. Critchfield, *J. Cellular Plast.*, **17**(6), 333 (1981).
8. V. V. Zarkov, L. I. Kopusov, and E. A. Petrov, "Cellular and Non-cellular Polyurethanes," International Conference, Strassbourg, France, Urethane Division, SPI, 1980, p. 635.
9. G. R. Rossmy, H. J. Kollmeier, W. Lidy, H. Schator, and M. Wiemann, *J. Cellular Plast.*, **13**(1), 26 (1977).
10. G. R. Rossmy, H. J. Kollmeier, W. Lidy, H. Schator, and M. Wiemann, *J. Cellular Plast.*, **17**(6), 319 (1981).
11. P. Van Gheluwe and J. LeRoux, *J. Appl. Polym. Sci.*, **28**, 2053 (1983).
12. R. L. Rowton, *J. Cellular Plast.*, **16**, 287 (1980).
13. H. J. Kollmeier, G. Burkhart, J. Kietsch, and H. Lammerting, *J. Cellular Plast.*, **20**(6), 410 (1984).
14. G. Rossmy, W. Lidy, H. Schator, M. Wiemann, and H. J. Kollmeier, *J. Cellular Plast.*, **15**(5), 276 (1979).
15. H. J. Kollmeier, H. Schator, and P. Zaeske, SPI 27th Annual Technical/Marketing Conference Proceedings, Bal Harbor, FL, 1982, p. 251.
16. R. W. Hendricks, *J. Appl. Crystallogr.*, **11**, 15 (1978).
17. NCSASR, "User Notes for the 10-Meter SAXS Instrument," ORNL, Oak Ridge, TN, 1983.
18. D. S. Huh and S. L. Cooper, *Polym. Eng. Sci.*, **11**(5), 369 (1971).
19. C. G. Seefried, J. V. Koleske, and F. E. Critchfield, *J. Appl. Polym. Sci.*, **19**, 2493 (1975).
20. C. G. Seefried, J. V. Koleske, and F. E. Critchfield, *J. Appl. Polym. Sci.*, **19**, 2503 (1975).
21. C. G. Seefried, J. V. Koleske, and F. E. Critchfield, *J. Appl. Polym. Sci.*, **19**, 3185 (1975).
22. C. S. Paik Sung, C. B. Hu, and C. S. Wu, *Macromolecules*, **13**, 111 (1980).
23. R. W. Seymour and S. L. Cooper, *Macromolecules*, **6**, 48 (1973).
24. D. Tyagi, Ph.D. Thesis, Virginia Polytechnic Institute and State University, Chemical Engineering Dept., Blacksburg, VA, 1985.
25. Y. P. Chang and G. L. Wilkes, *J. Polym. Sci., Polym. Phys. Ed.*, **13**, 455 (1975).
26. N. S. Schneider, C. S. Paik Sung, R. W. Matton, and J. L. Illinger, *Macromolecules*, **8**(1), 62 (1975).
27. R. Bonart, L. Morbitzer, and E. H. Muller, *J. Macromol. Sci. Phys.*, **B9**(3), 447 (1974).
28. O. Glatters and O. Kratky, Eds., *Small Angle X-Ray Scattering*, Academic, New York, 1982.
29. G. L. Wilkes and S. Abouzahr, *Macromolecules*, **14**, 458 (1981).
30. J. T. Koberstein and R. S. Stein, *J. Polym. Sci., Polym. Phys. Ed.*, **21**, 1439 (1983).
31. G. Porod, *Kolloid Z.*, **124**, 83 (1951).
32. G. Porod, *Kolloid Z.*, **125**, 51 (1952).
33. G. Porod, *Kolloid Z.*, **125**, 108 (1952).
34. E. Helfand, *Acc. Chem. Res.*, **8**, 295 (1975).
35. E. Helfand and Y. Tagami, *Polym. Lett.*, **9**, 741 (1971).
36. J. T. Koberstein, B. Morra, and R. S. Stein, *J. Appl. Crystallogr.*, **13**, 34 (1980).
37. J. T. Koberstiein and R. S. Stein, *Polymer, Eng. Sci.*, **24**(5), 293 (1984).

Received January 22, 1987
Accepted May 28, 1987